A Long-Lived Fluorenyl Cation: Efficiency Booster for Uncaging and Hydroxide Emission

Chahinez Abdellaoui,[a] Volker Hermanns,[b] Matiss Reinfelds,[b,c] Maximilian Scheurer,[d] Andreas Dreuw,[d] Alexander Heckel [b] and Josef Wachtveitl *[a]

a. Institute of Physical and Theoretical Chemistry, Goethe-University Frankfurt, Frankfurt am Main 60438, Germany. E-mail: abdellaoui@theochem.uni-frankfurt.de; wveitl@theochem.uni-frankfurt.de

b. Institute of Organic Chemistry, Goethe-University Frankfurt, Frankfurt am Main 60438, Germany. E-mail: Hermanns@chemie.uni-frankfurt.de; Heckel@chemie.uni-frankfurt.de

c. Institute of Chemistry and Technology of Materials (ICTM), NAWI Graz, Graz University of Technology, Graz 8010, Austria. E-mail: reinfelds@tugraz.at;

d. Interdisciplinary Center for Scientific Computing, Heidelberg University, Heidelberg 69120, Germany. E-mail: maximilian.scheurer@iwr.uni-heidelberg.de; andreas.dreuw@iwr.uni-heidelberg.de.

Content

Experimental

The sample was first constantly illuminated with **LEDs** (Thorlabs GmbH) at 365 nm (M365L2, FWHM: 7.5 nm) with 2.9 mW and 300 nm (M300L4, FWHM: 20 nm) with 0.7 mW. All UV/vis measurements and pH-Experiments were measured in 1.0 cm quartz fluorescence cuvette (QS) from Hellma-Analytics.

For the **UV/vis measurements** the spectra were recorded with a Specord S600 spectrophotometer (Analytik Jena) every 30 s for the first hour, afterwards every 60 s. The LEDs were placed approximately 1 cm from the sample.

The **IR spectra** were recorded with a FTIR spectrometer Vertex 80 (Bruker, Ettlingen) every 60 s under constant nitrogen flow. The sample chamber was continuously purged with nitrogen so that the influence of water vapour and carbon dioxide on the IR measurement is minimised. Measurements were made in the wavenumber range from 4000 cm^{-1} to 800 cm^{-1} with a resolution of 2 cm^{-1}. The LED was placed at a distance of approximately 20 cm from the sample, and a mirror was used to guide the excitation beam on the sample. The samples were placed in a sandwich cuvette with calcium fluoride (CaF_2) windows and a 50 µm spacer made of polytetrafluoroethylene (PTFE). The evaluation of the measured spectra was partly carried out with the programme OPUS from Bruker.

Flash photolysis measurements were performed using a Nd:YAG laser (SpitLight 600, Innolas Laser) pumping an optical parametric oscillator (preciScan, GWU-Lasertechnik). For generation of the pump pulse the OPO was set to 355 nm with a power of 2 mJ. The probe pulse was generated by a mercury-xenon flashlamp (LC8, Hamamatsu) and then selected by two monochromators (Photon Technology International). For the detection the transient signal was guided through a photomultiplier tube (H6780-02, Hamamatsu) and recorded with an oscilloscope (DPO5204-10RL, Tektronix). The measurements were performed in a time rage between 1 µs and 1 s (respectively 0.001 s and 1000 s). At each time point spectra were 20 times averaged. A 2x10 mm quartz cuvette was used for this type of measurements.

For the **Femtosecond absorption measurements,** a Clark MXR-CPA-Series (Horiba GmbH) was used as a laser system with fundamental wavelength of 775 nm, 1 kHz repetition rate and 150 fs pulse width. The pump pulse was converted from the fundamental wavelength by a difference frequency generation, resulting in 315 nm and 90 nJ excitation power. For the probe pulse a CaF_2 window was used to generate a supercontinuum white light from around 320 nm to 690 nm. To avoid any anisotropic effects, the polarization angle between pump und probe pulse was set to 54.7°. The data analysis was carried out with the program OPTIMUS.[1] A global life analysis (GLA) was used, where a fixed set of exponential functions was used to fit all transients.

NMR spectra were measured on a Bruker AV 400 device. Deuterated solvents (purchased at Eurisotop) were used for sample preparation. Spectra were referenced to the solvent peak. The used value is: DMSO-d_6 ^{1}H 2.50. Chemical shifts (δ) are reported on a ppm scale. The following abbreviations (or combinations thereof) were used to describe multiplicities: s = singlet, d = doublet. Coupling constants (J) are reported in Hertz (Hz).

Mass spectrometry was performed on ThermoFisher Surveyor MSQ™ (ESI - Electrospray ionization) device from Thermo Fisher Scientific.

Irradiation experiments were done in 1.0 cm quartz fluorescence cuvette (QS) from Hellma-Analytics equipped with a magnetic stirrer. Light sources (365 nm, LED M365L2) were operated by DC2100 LED driver (from Thorlabs) in external trigger mode. The external trigger was provided by an in-house programmed software PHITS.

For **high-performance liquid chromatography** an Agilent Technologies 1260 Infinity instrument was used, equipped with quaternary pump, automatic liquid sampler, thermostatted column compartment and diode array detector. Separation was done using MultoKrom® 100-5 C18 column (250 x 4.6 mm) from CS-Chromatographie Service GmbH. Binary solvent mixtures were used for elution. Typical gradients are described in Table S1 and shown in Figure S20.

UV/vis steady state measurements

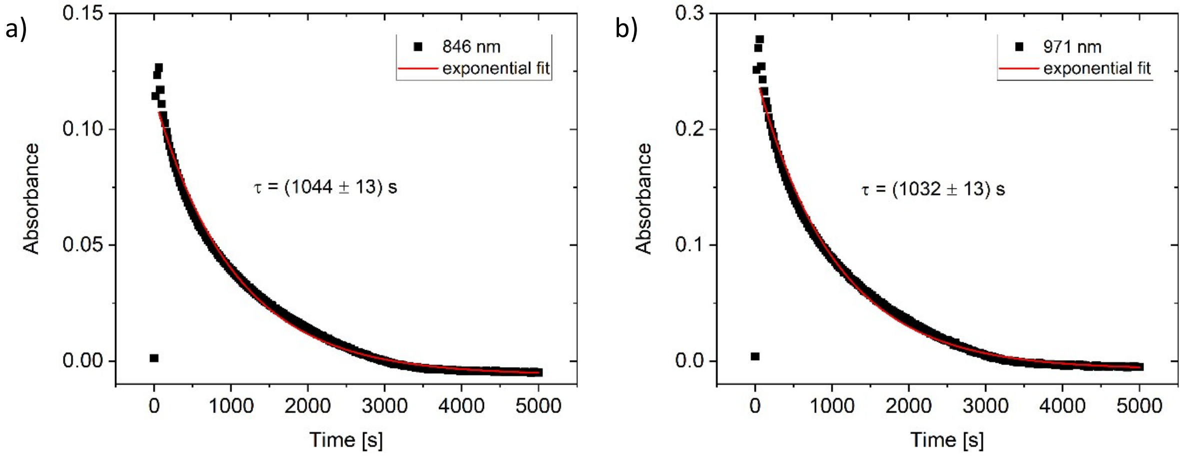

Figure S1: Time-resolved thermal response of the cation at 846 nm (a) and 971 nm (b) generated from the sample $(DMA)_2$F-OH in MeOH and the corresponding exponential fits (red lines).

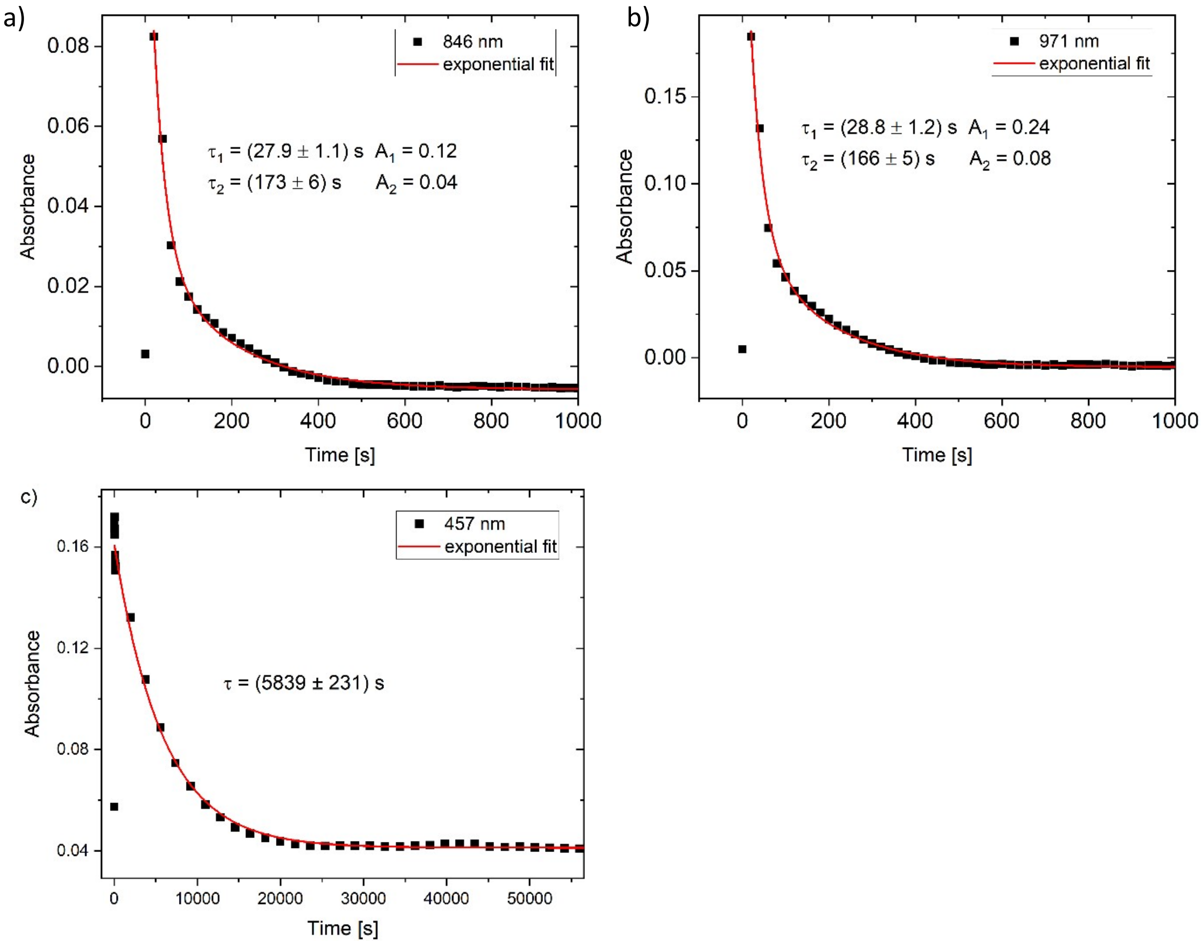

Figure S2: Time-resolved thermal response of the cation at 846 nm (a) and 971 nm (b) generated from the sample $(DMA)_2$F-OH in EtOH and in H_2O (c) and the corresponding exponential fits (red lines).

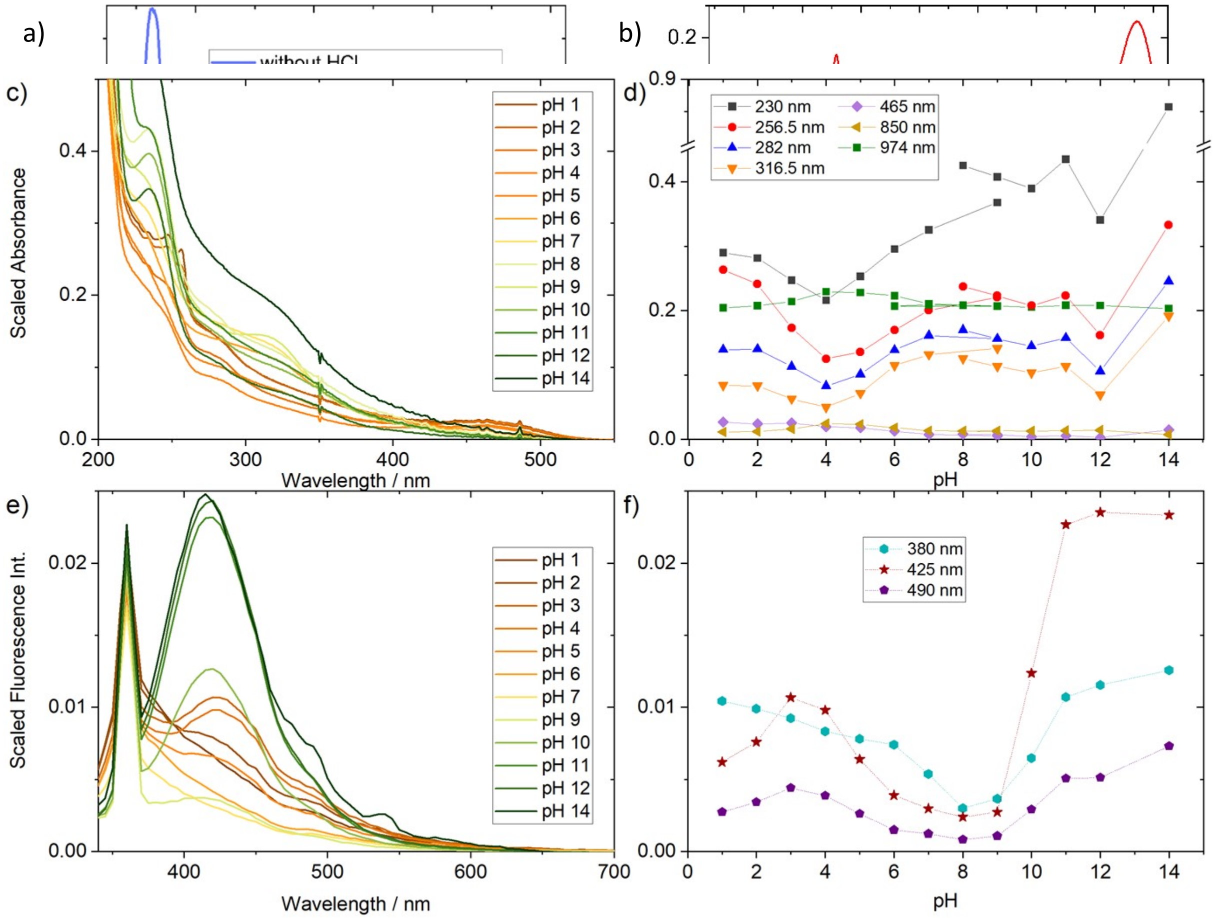

Figure S3: (a) Absorption spectra $(DMA)_2$F-Ac in MeOH before and after different amounts of 0.1 M HCl (without illumination). (b) Difference spectra of $(DMA)_2$F-Ac after 1 minute of illumination at 365 nm (red line) and after addition of 1 eq HCl in H_2O (brown line). Absorption (c) and Fluorescence spectra (d) of $(DMA)_2$F-OH in H_2O during the titration from pH 6 to pH 1 with HCl (without illumination) and from pH 6 to pH 14 with NaOH and the evolution of selected Wavelengths (e, f) of the corresponding measurements.

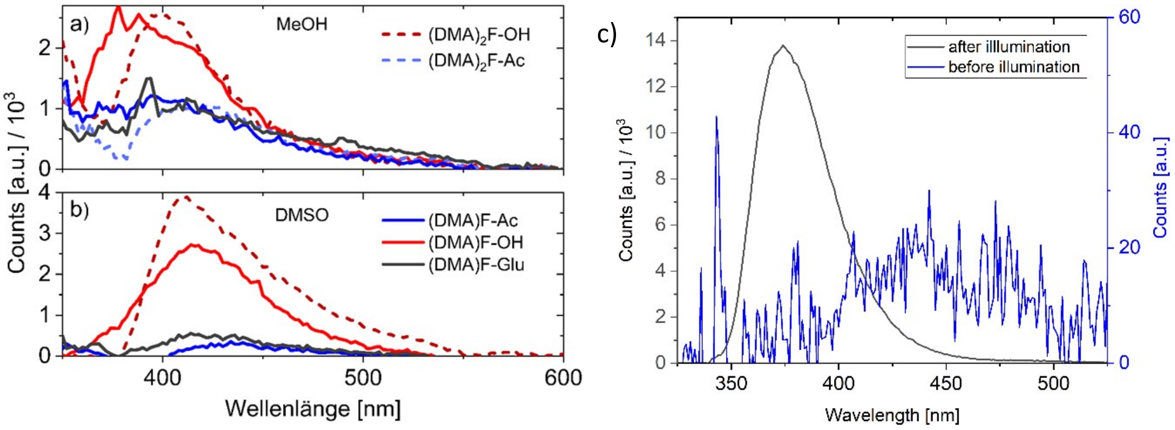

Figure S4: Fluorescence spectra of all derivatives in MeOH (a) and DMSO (b) at 365 nm excitation. c) Flouorescence spectra of $(DMA)_2$F-OH in MeOH without (black) and with previous illumination (1 min, blue).

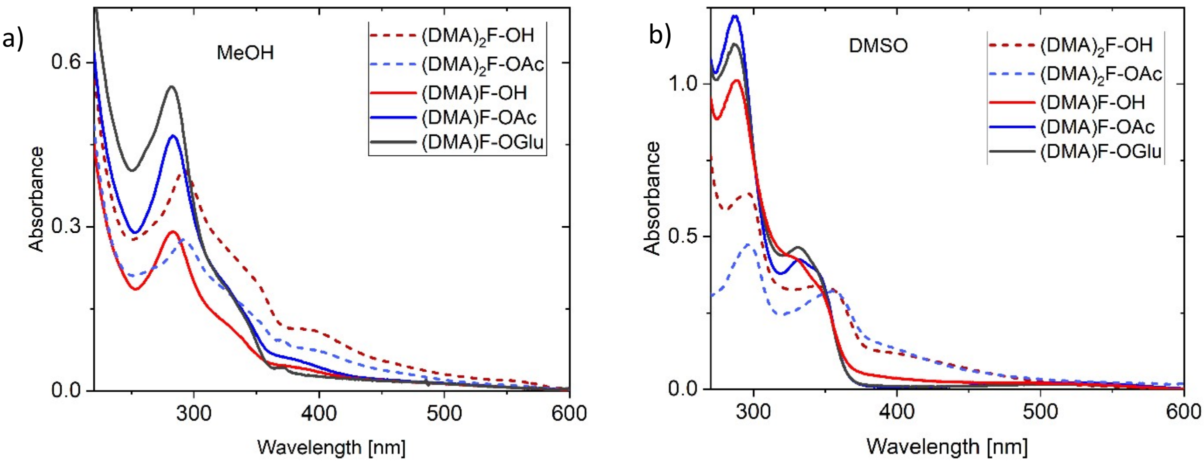

Figure S5: Absorption spectra of all derivatives after continuous illumination at 365 nm in MeOH (a) and DMSO (b).

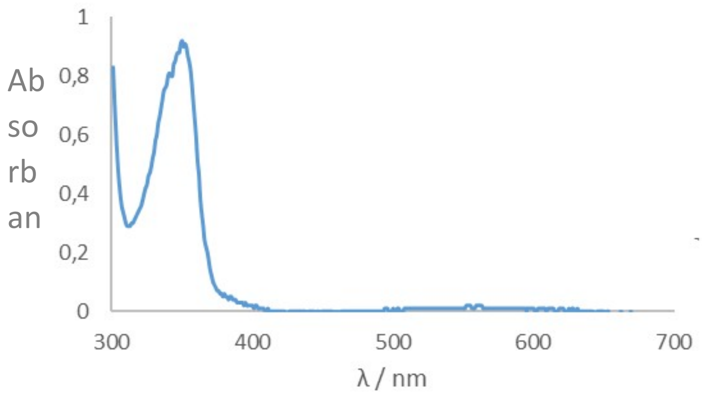

Figure S6: Absorption spectra of symmetric fluorenone $(DMA)_2F{=}O$ in acetonitrile (MeCN).

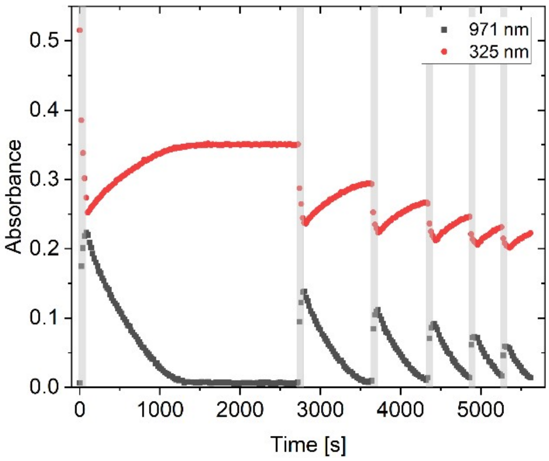

Figure S7: Temporal evolution of $(DMA)_2F$-OH sample at 325 nm (red dots) and 971 nm (black dots) starting with 100 s of illumination (light grey area) followed by non-illuminated data points.

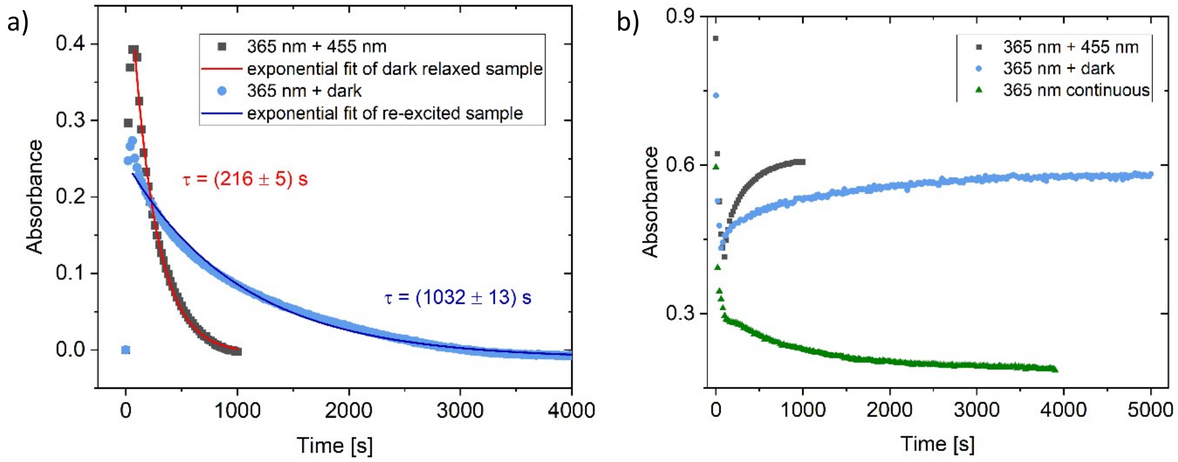

Figure S8: Time resolved response of $(DMA)_2F$-OH sample at 971 nm (a) and 325 nm (b) with re-excitation of the cation at 455 nm (black dots), without further illumination of the cation (blue dots) and with continuous illumination at 365 nm (green dots): first data point: signal from starting material; (subsequent 3 data points: during excitation at 365 nm).

FTIR steady state measurements

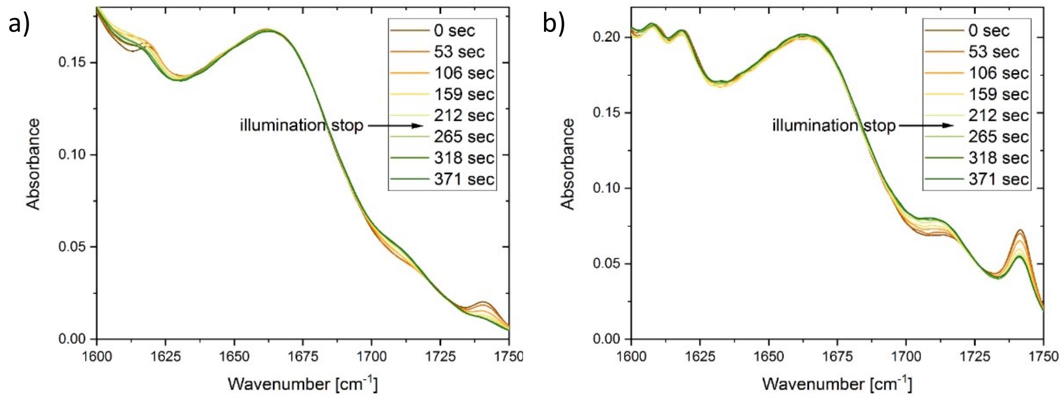

Figure S9: FTIR spectra of $(DMA)_2F$-OAc (a) and (DMA)F-OAc (b) in MeOH: first spectrum is of starting material (without illumination), next four spectra with 300 nm illumination (53 s – 212 s) and the subsequent three spectra without illumination (265 s – 371 s).

Ultrafast UV/vis measurements

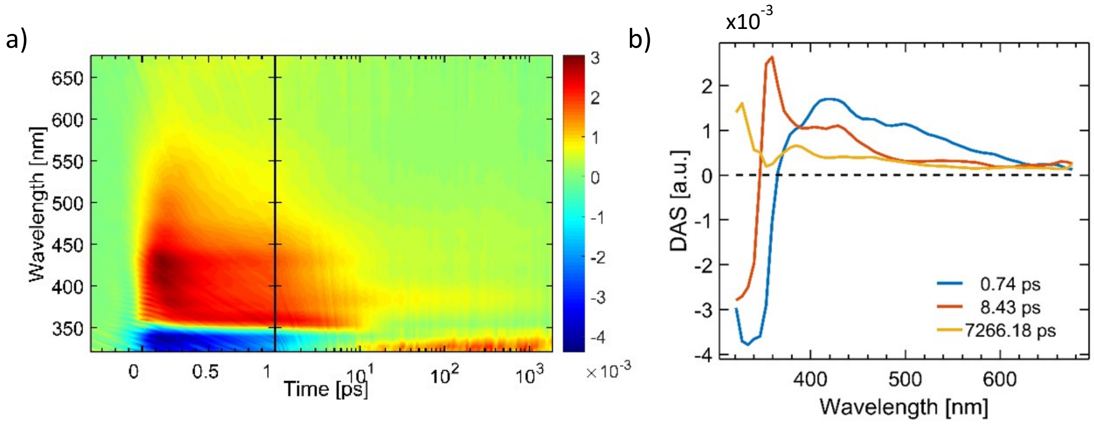

Figure S10: Transient UV/vis spectra of $(DMA)_2F$-Ac in MeOH with 90 nJ excitation power at 315 nm (a) and corresponding decay associated spectra (b).

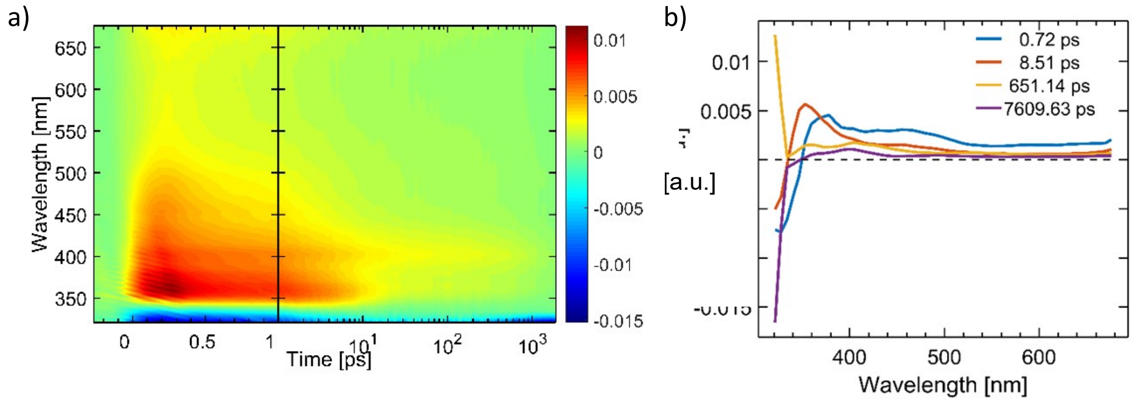

Figure S11: Transient UV/vis spectra of (DMA)F-Ac in MeOH with 90 nJ excitation power at 315 nm (a) and corresponding decay associated spectra (b).

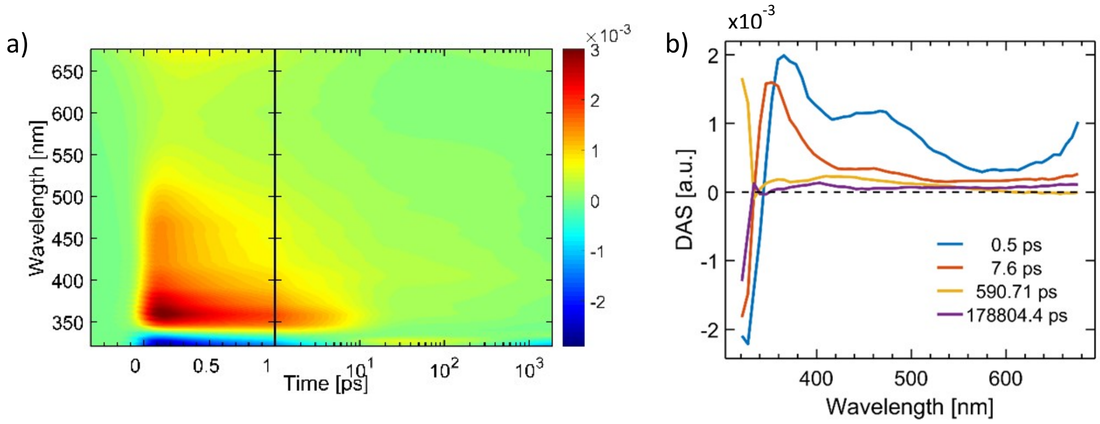

Figure S12: Transient UV/vis spectra of (DMA)F-Glu in MeOH with 90 nJ excitation power at 315 nm (a) and corresponding decay associated spectra (b).

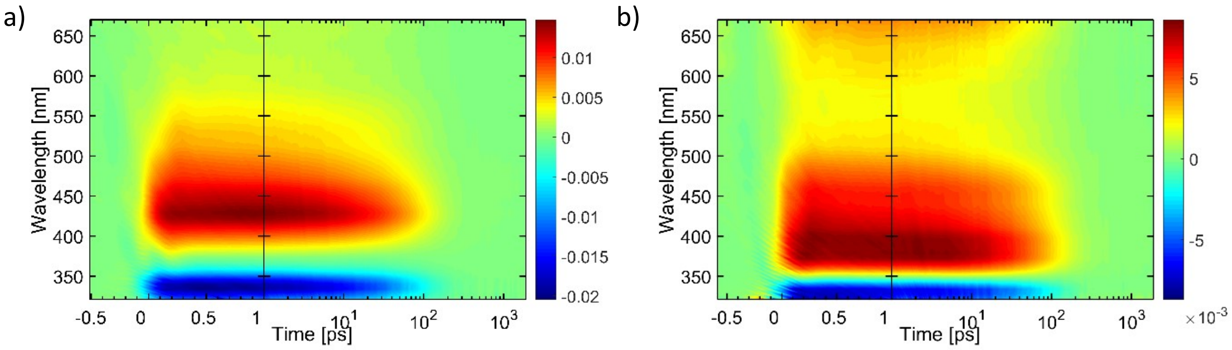

Figure S13: Transient UV/vis spectra of $(DMA)_2$F-OH (a) and (DMA)F-OH (b) in DMSO with 90 nJ excitation power at 315 nm.

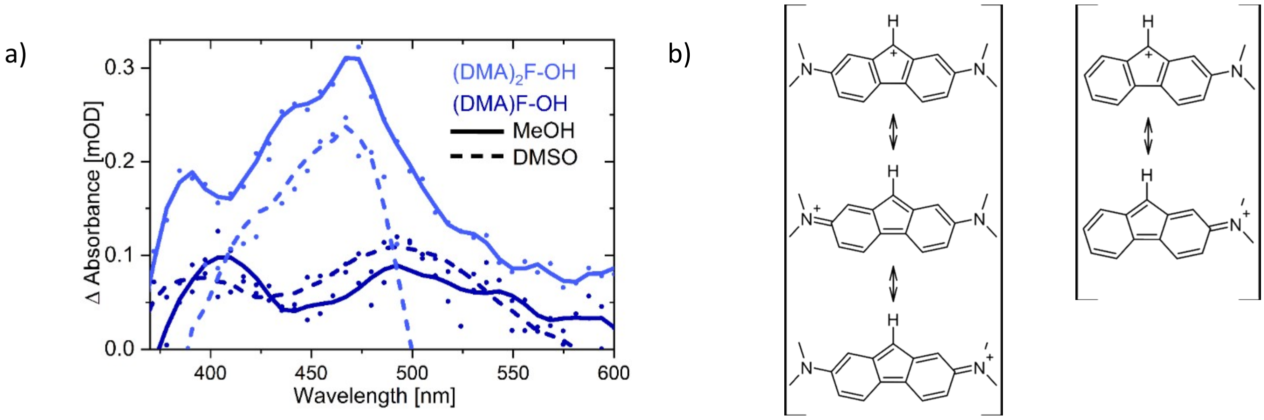

Figure S14: (a) Spectra of (DMA)$_2$F-OH (light blue) and (DMA)F-OH (dark blue) in MeOH (solid line) and DMSO (dashed line) at 1900 ps after excitation obtained from the transient UV/vis-measurements. (b) Mesomeric resonance structure of (DMA)$_2$F$^+$ and (DMA)F$^+$.

UV/vis flash photolysis measurements

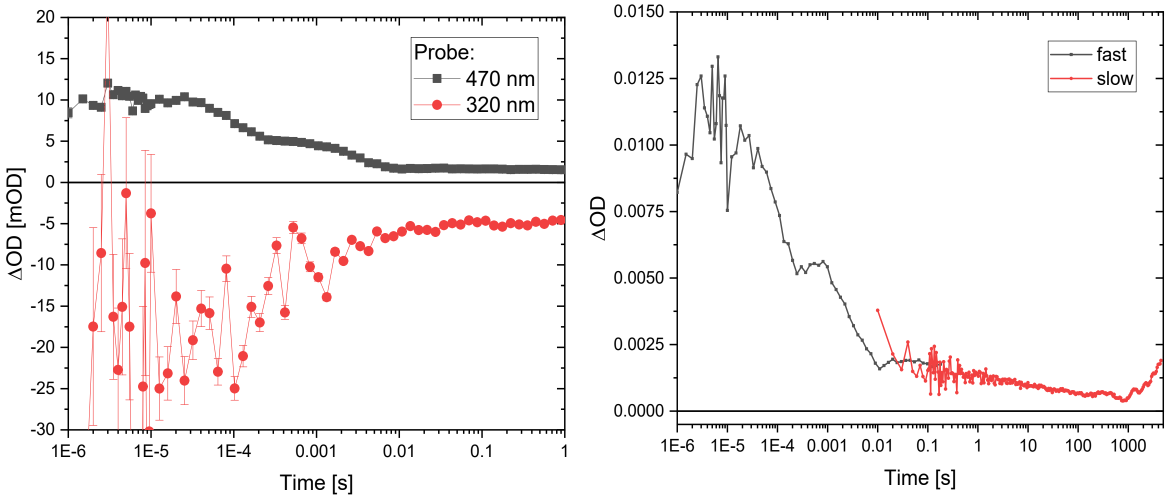

Figure S15: Flash photolysis data of (DMA)$_2$F-OH in MeOH at 470 nm and 320 nm (a) and 460 nm for longer time range (b)

Quantum Chemical Calculations

UV/Vis Spectra

All geometry optimizations were performed with Gaussian 16.[2] Molecular structures were optimized at the B3LYP/cc-pVDZ[3–5] level of theory employing a polarizable continuum model (PCM) with methanol as solvent.[6,7] Ten singlet excited states were computed using time-dependent density functional theory (TDDFT) as implemented in Gaussian 16 at the same level of theory including contributions from the solvent through a linear response (LR) formalism.[8] To reliably confirm the identity of the suspected cationic species with an *ab-initio* wave function approach, the five energetically lowest singlet excited states of these species ((DMA)$_2$F-cation and (DMA)F-cation) were computed with LR-PCM-ADC(2)/cc-pVDZ using PySCF in combination with adcc.[9–11] The obtained stick spectra were convoluted using Gaussian functions with a standard deviation of 0.333 eV.

IR Spectra

The vibrational modes were calculated after geometry optimization at the B3LYP/cc-pVDZ level of theory. IR spectra were obtained by convoluting the stick spectra with Gaussian functions with a standard deviation of 4 cm^{-1}.

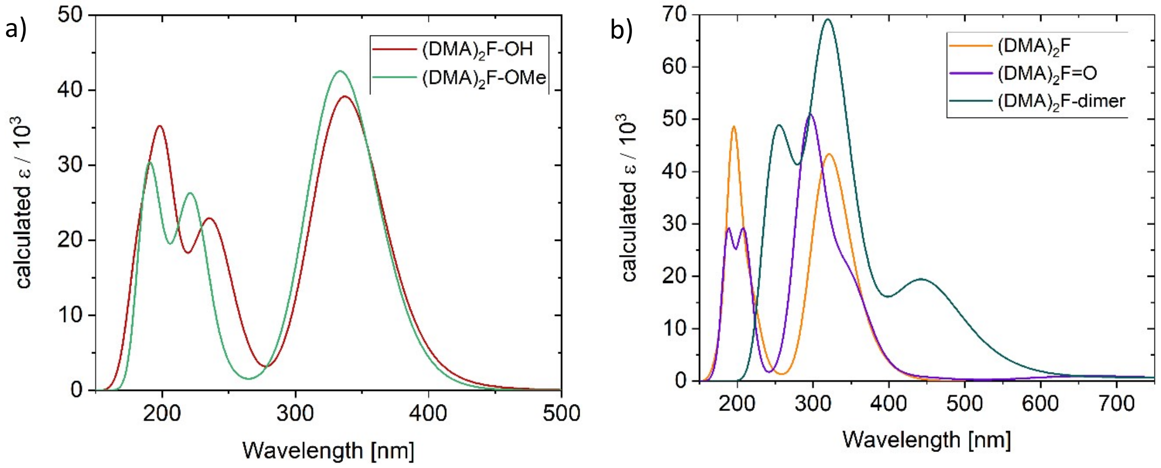

Figure S16: Computed spectra of (a) (DMA)$_2$F-OH and (DMA)$_2$F-OMe and (b) the photoproducts (DMA)$_2$F, (DMA)$_2$F=O and (DMA)$_2$F-dimer at the B3LYP/cc-pVDZ level of theory employing LR-PCM with methanol as solvent.

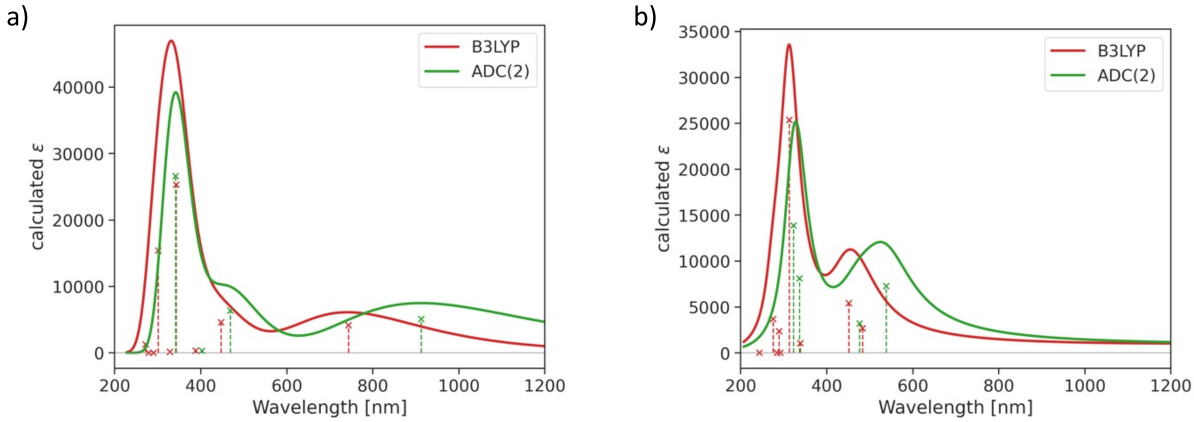

Figure S17: Computed spectra of $(DMA)_2F$-cation (a) and (DMA)F-cation (b) in methanol using TD-B3LYP and ADC(2) with a LR-PCM formalism.

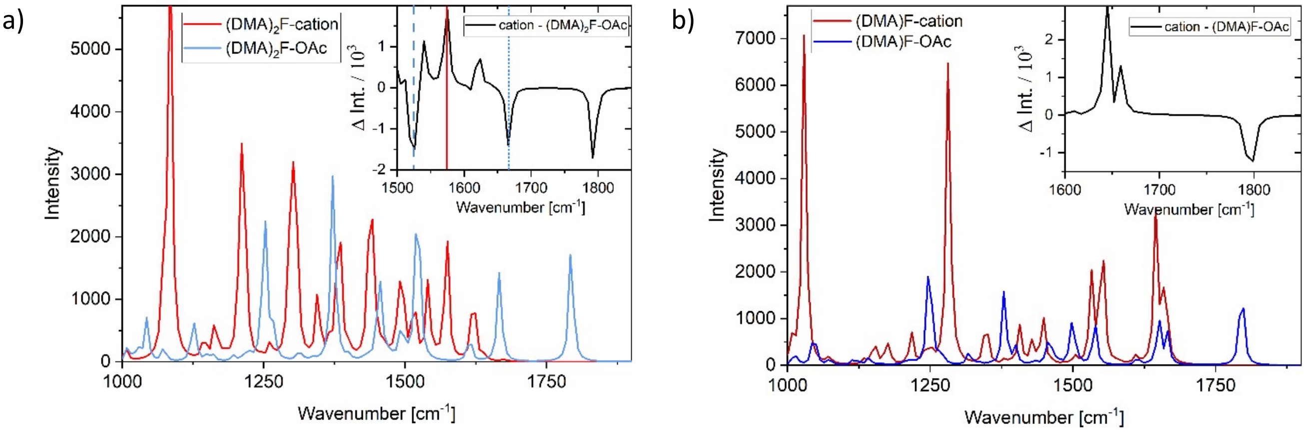

Figure S18: (a) Computed IR-spectra of $(DMA)_2F$-OAc (light blue), the symmetric cation (red) and the difference spectrum (inset). (b) Computed IR-spectra of (DMA)F-OAc (blue), the symmetric cation (dark red) and the difference spectrum (inset).

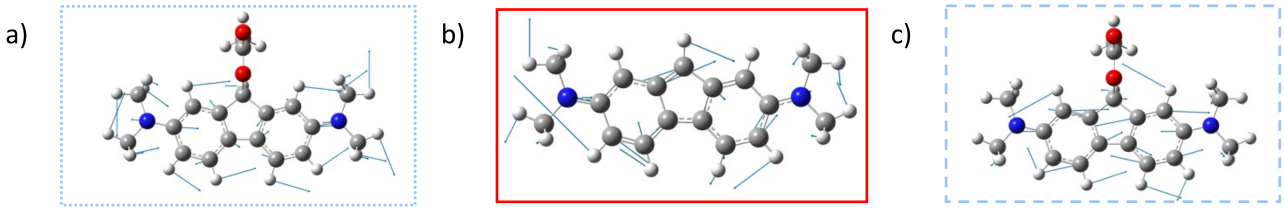

Figure S19: Illustrations of the displacement vectors for the vibrational modes of (a) $(DMA)_2F$-OAc at 1522 cm^{-1} and (c) 1666 cm^{-1} and (b) the $(DMA)_2F$-cation at 1573 cm^{-1}.

Synthesis

Synthesis of $(DMA)_2$-fluorenon as reference compound.

286 mg (1.07 mmol, 1 eq) 2,7-bis(dimethylamino)-9H-fluoren-9-ol were solved in 10 ml CH_2Cl_2 and 497 mg (1.17 mmol, 1.1 eq) Dess-Martin-Periodinan were added. After 30 minutes of stirring at room temperature, the reaction mixture was diluted with $NaHCO_3$. The mixture was extracted four-times with ethyl acetate, and the organic phase was dried over Na_2SO_4. Now the solvent was removed under reduced pressure. The chromatographic purification was performed isocratic with a solvent mixture of 19:1 (DCM:MeOH). The product was obtained as a dark solid.

Yield: 94 mg (0.35 mmol, 33%)
^{1}H-NMR (400 MHz, DMSO-d_6): δ 7.33 (d, ^3J = 8.06 Hz, 2H), 6.86 (d, ^4J = 2.56 Hz, 2H), 6.79 (dd, ^3J = 8.06 Hz, ^4J = 2.56 Hz, 2H), 2.94 (s, 12H) ppm.

ESI-MS [m/z]: calc. for $[C_{17}H_{18}N_2O]+H^+$: 267.15 found: 267.34.

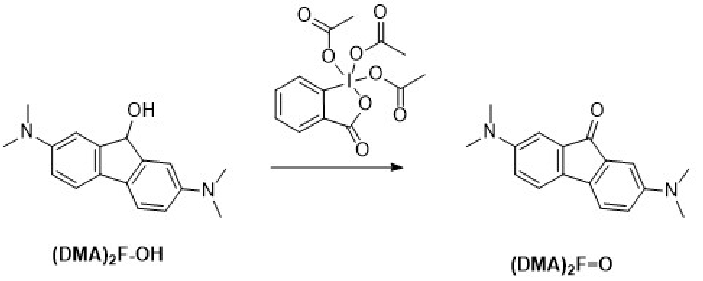

Scheme S1: Structure of $(DMA)_2F{=}O$

Photoproduct Identification

Table S1: HPLC-solvent gradients used for identification of the photo products.

Gradient 1	
Time (min)	Solvent A (%)
0 to 5	5

5 to 15	5 to 40
15 to 45	40 to 60
45 to 50	60 to 100
50 to 54	100

Gradient 1: Solvent A – MeCN; solvent B – ultra pure water + 0.1% TFA

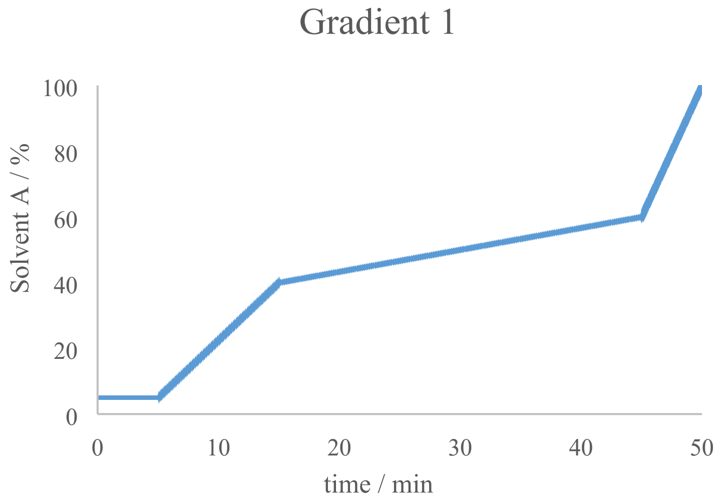

Figure S20: HPLC gradient used for separation of the photoproducts after irradiation experiments.

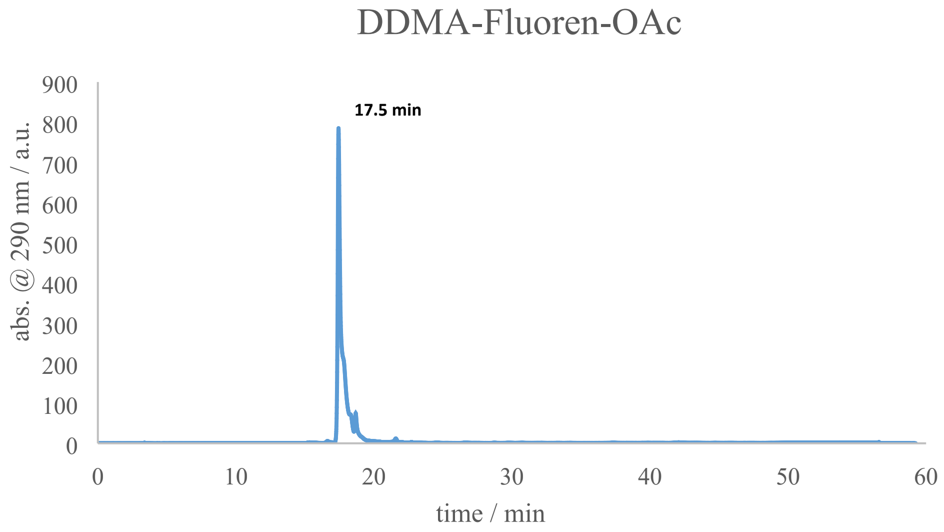

Figure S21: HPLC chromatogram of $(DMA)_2F$-OAc before irradiation.

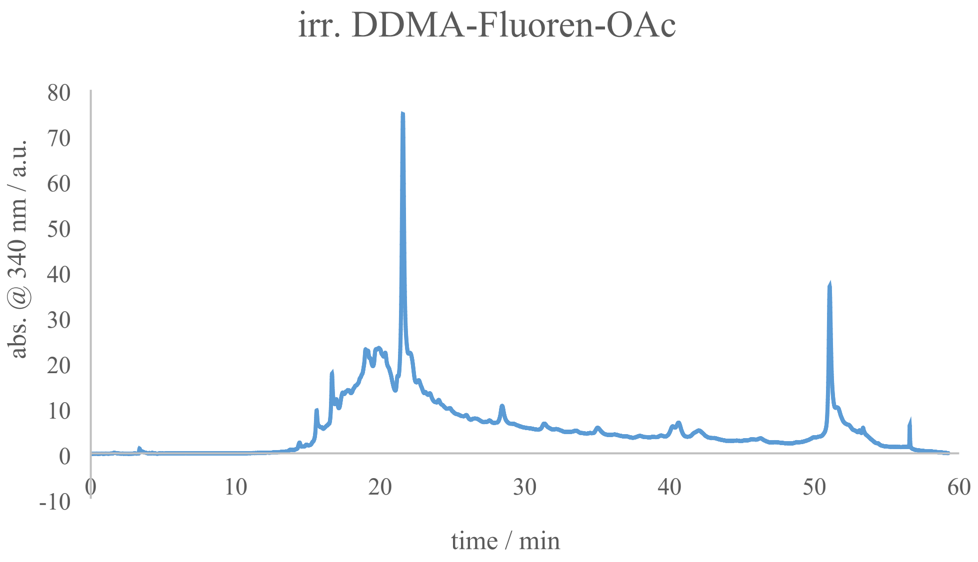

Figure S22: HPLC chromatogram of $(DMA)_2F$-OAc after irradiation for 40 min at 365 nm.

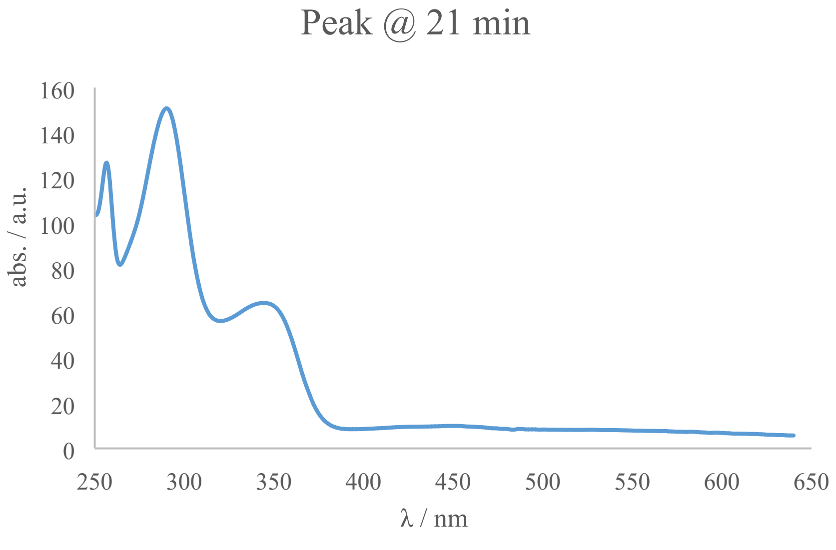

Figure S23: Absorbance spectrum at 21 minutes.

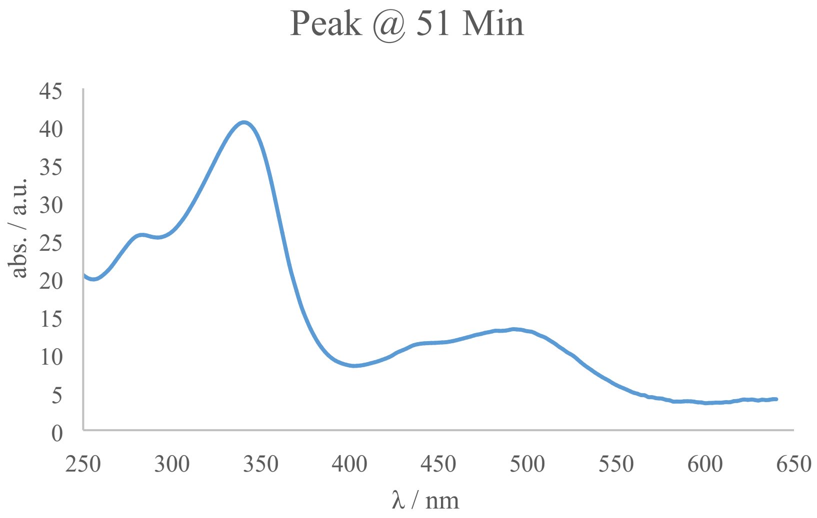

Figure S24: Absorbance spectrum at 51 minutes.

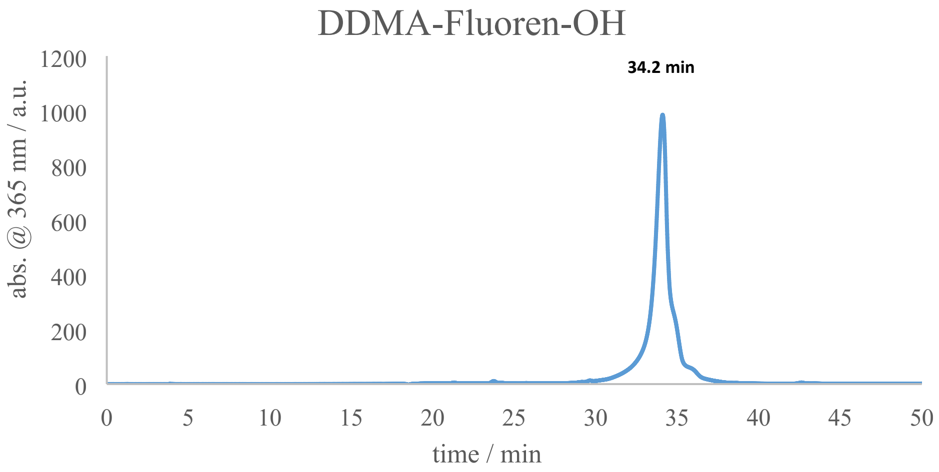

Figure S25: HPLC chromatogram of $(DMA)_2F$-OH before irradiation.

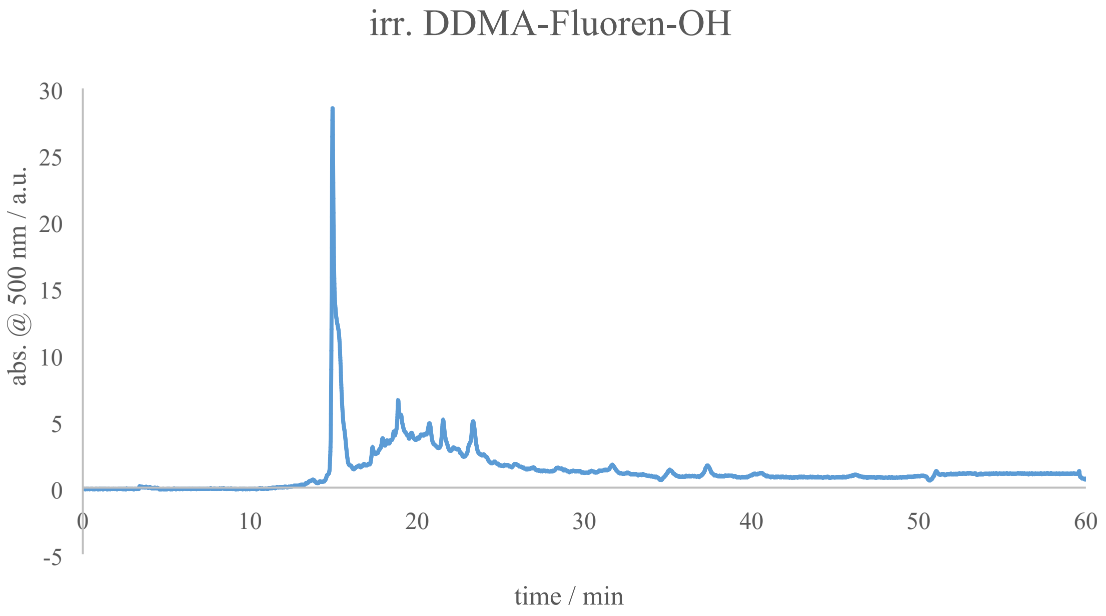

Figure S26: HPLC chromatogram of $(DMA)_2F$-OH after irradiation for 40 min at 365 nm.

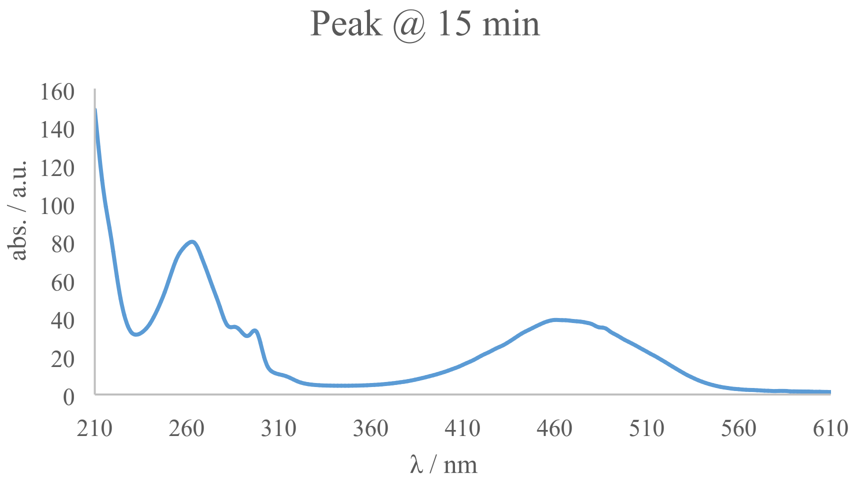

Figure S27: Absorbance spectrum at 15 minutes.

NMR spectra

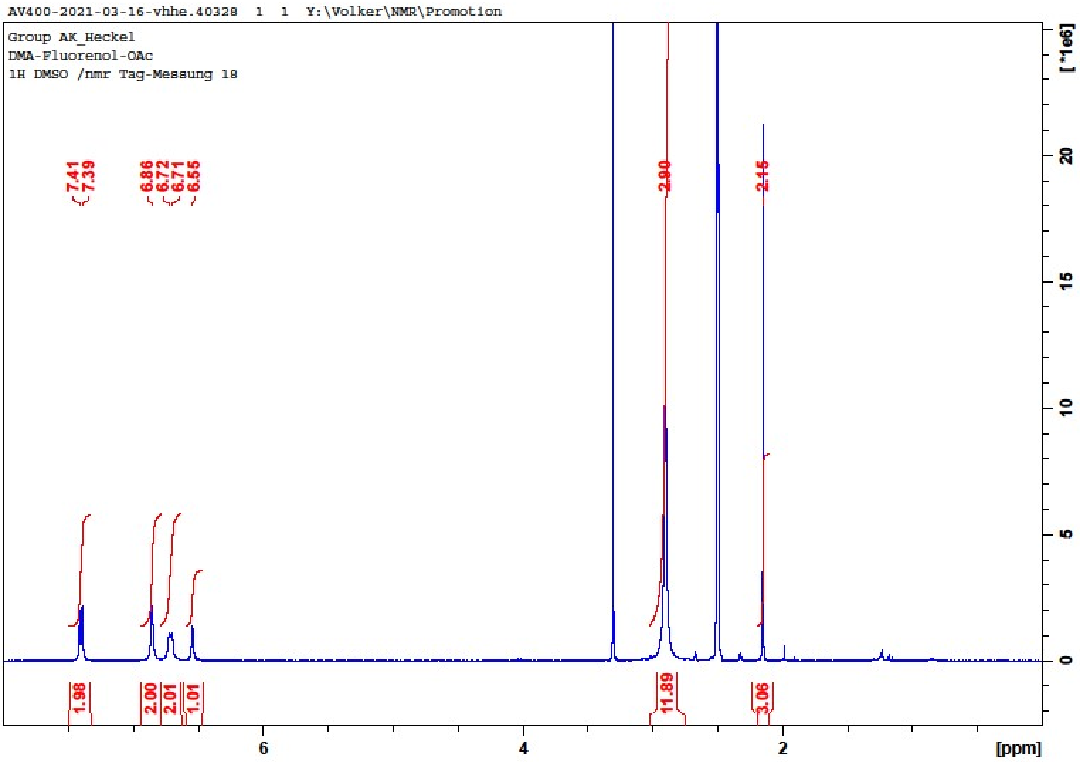

Figure S28: ^{1}H spectrum of $(DMA)_2$F-OAc before irradiation in DMSO-d_6.

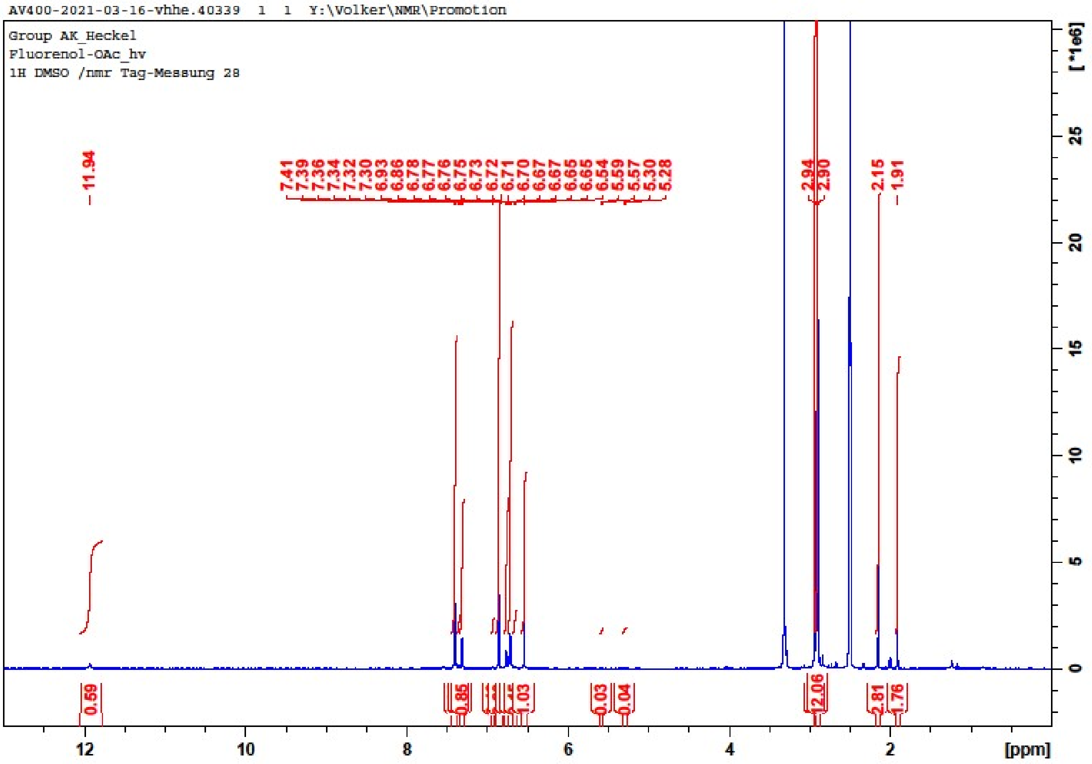

Figure S29: ^{1}H spectrum of $(DMA)_2$F-OAc after irradiation for 60 min at 365 nm in DMSO-d_6.

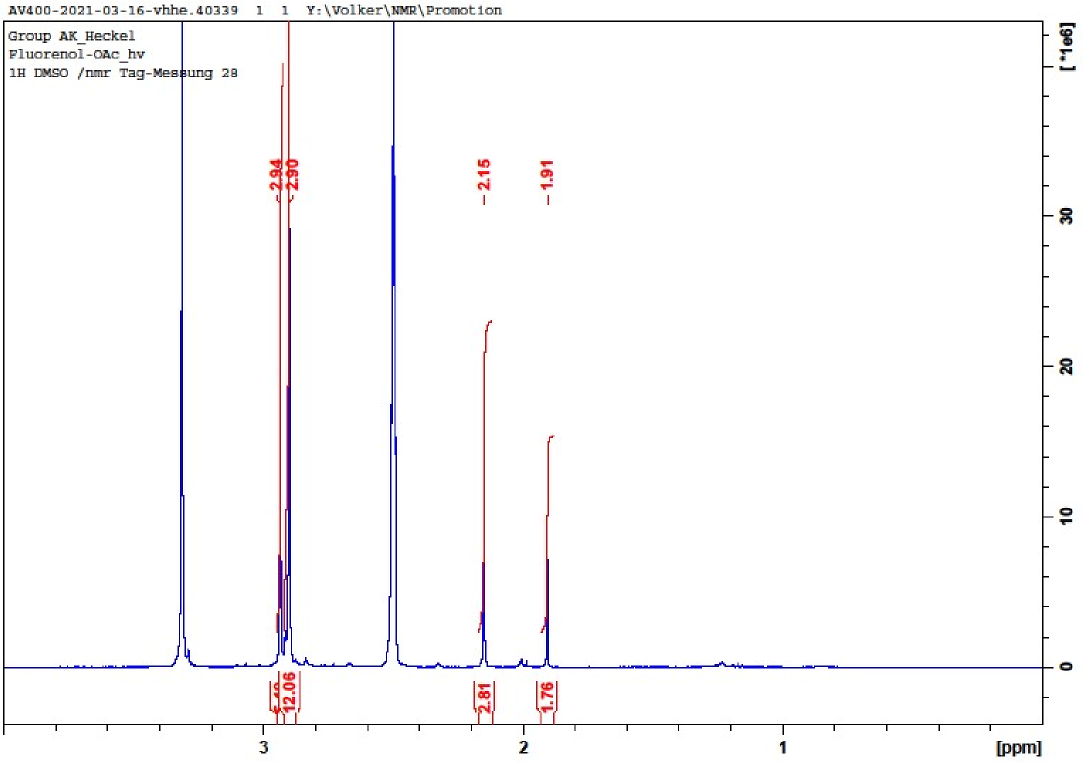

F

igure S30: ^{1}H spectrum of $(DMA)_2$F-OAc after irradiation in DMSO-d_6 (Zoom from 0 ppm to 4 ppm).

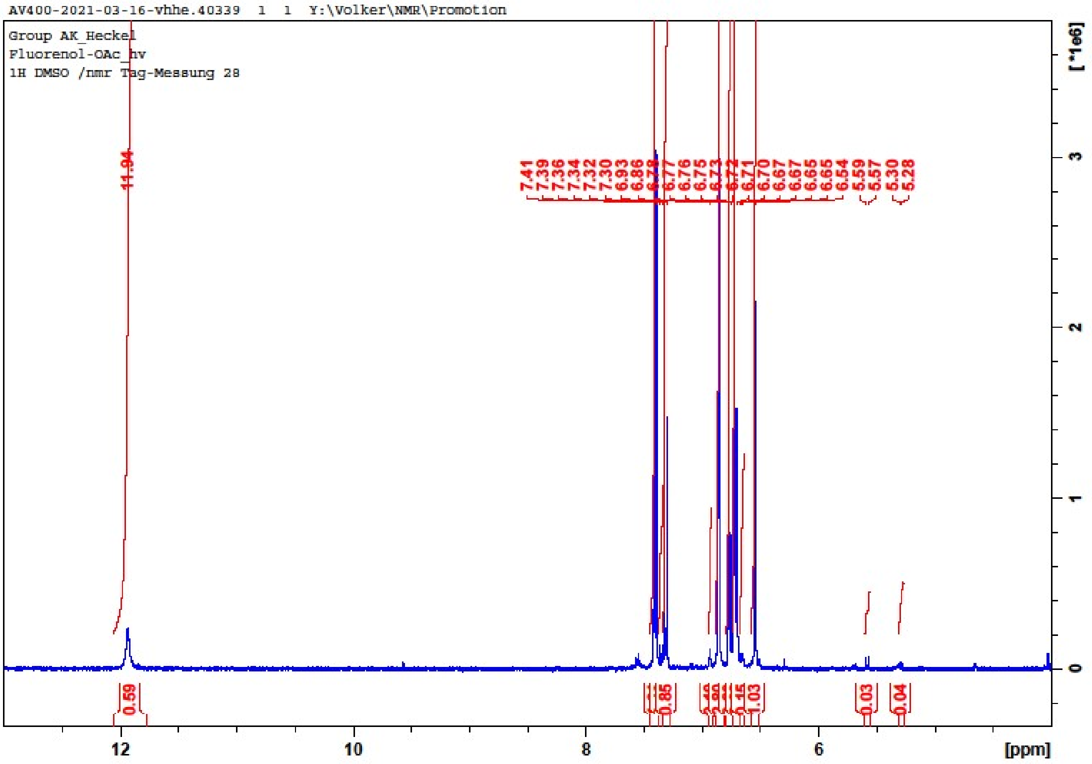

Figure S31: ^{1}H spectrum of (DMA)$_2$F-OAc after irradiation in DMSO-d$_6$ (Zoom from 4 ppm to 13 ppm).

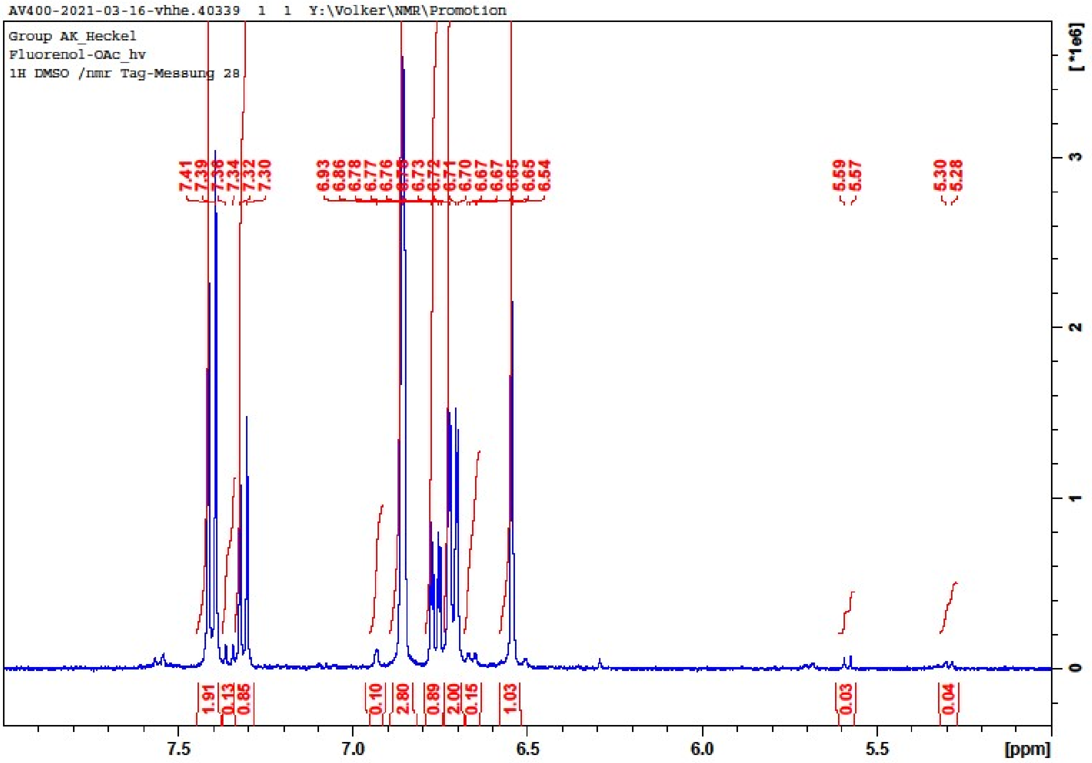

Figure S32: ^{1}H spectrum of (DMA)$_2$F-OAc after irradiation in DMSO-d$_6$ (Zoom from 5 ppm to 8 ppm).

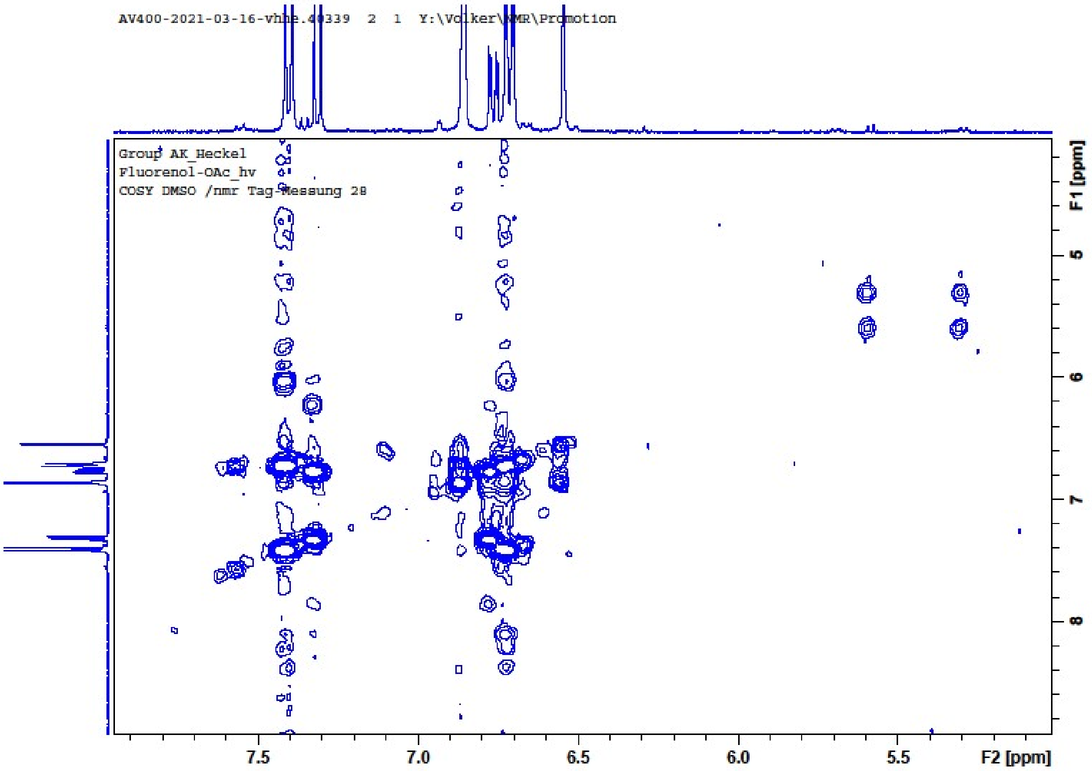

Figure S33: 2D-COSY-spectrum of $(DMA)_2F$-OAc after irradiation in DMSO-d_6 (Zoom from 5 ppm to 8 ppm).

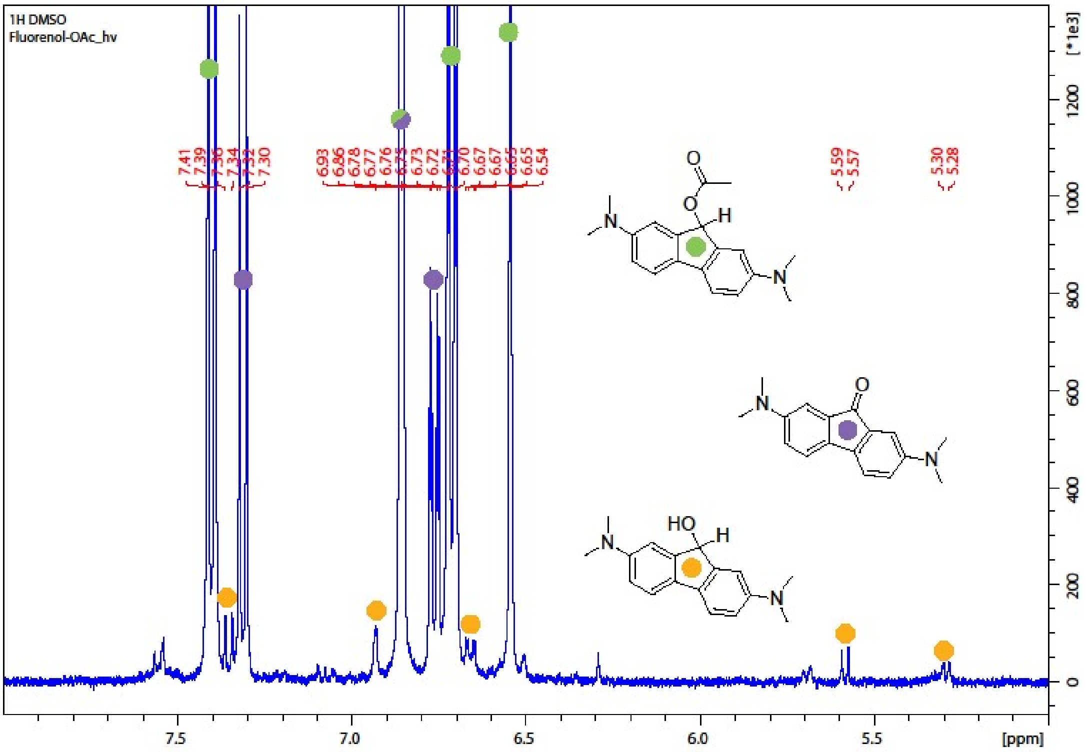

Figure S34: ^1H spectrum of $(DMA)_2F$-OAc after irradiation in DMSO-d_6 and respective photoproducts (Zoom from 5 ppm to 8 ppm).

Mass spectra

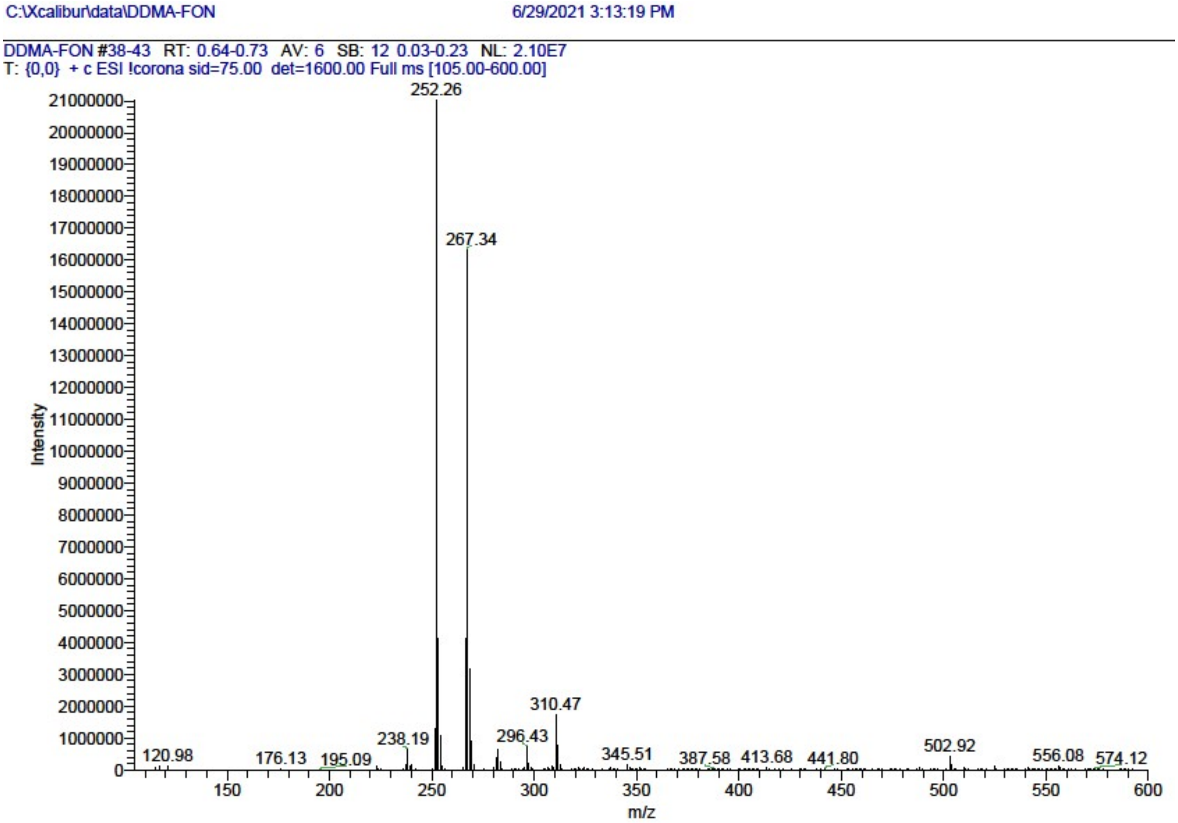

Figure S35: ESI mass spectrum of the reference compound $(DMA)_2F{=}O$.

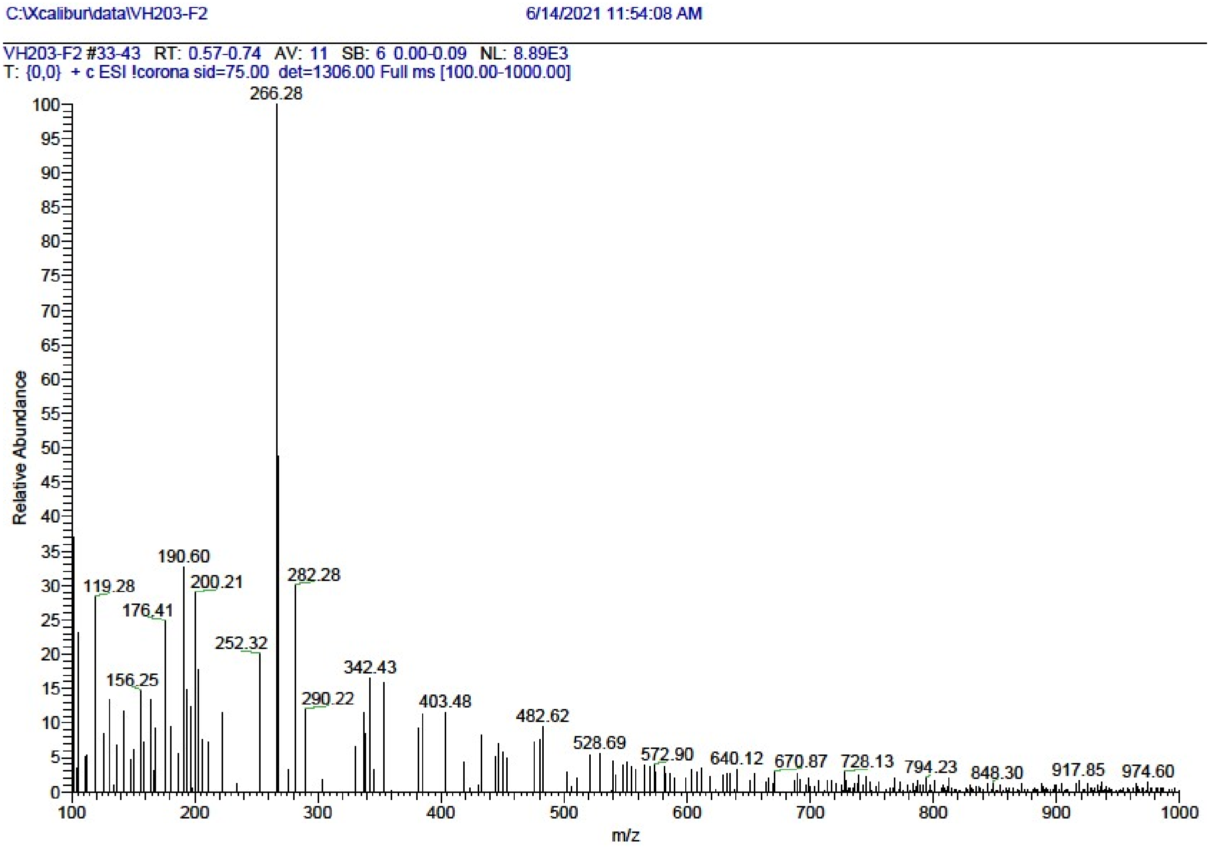

Figure S36: ESI mass spectrum of the photoproduct of (DMA)$_2$F-OAc at 21 min.

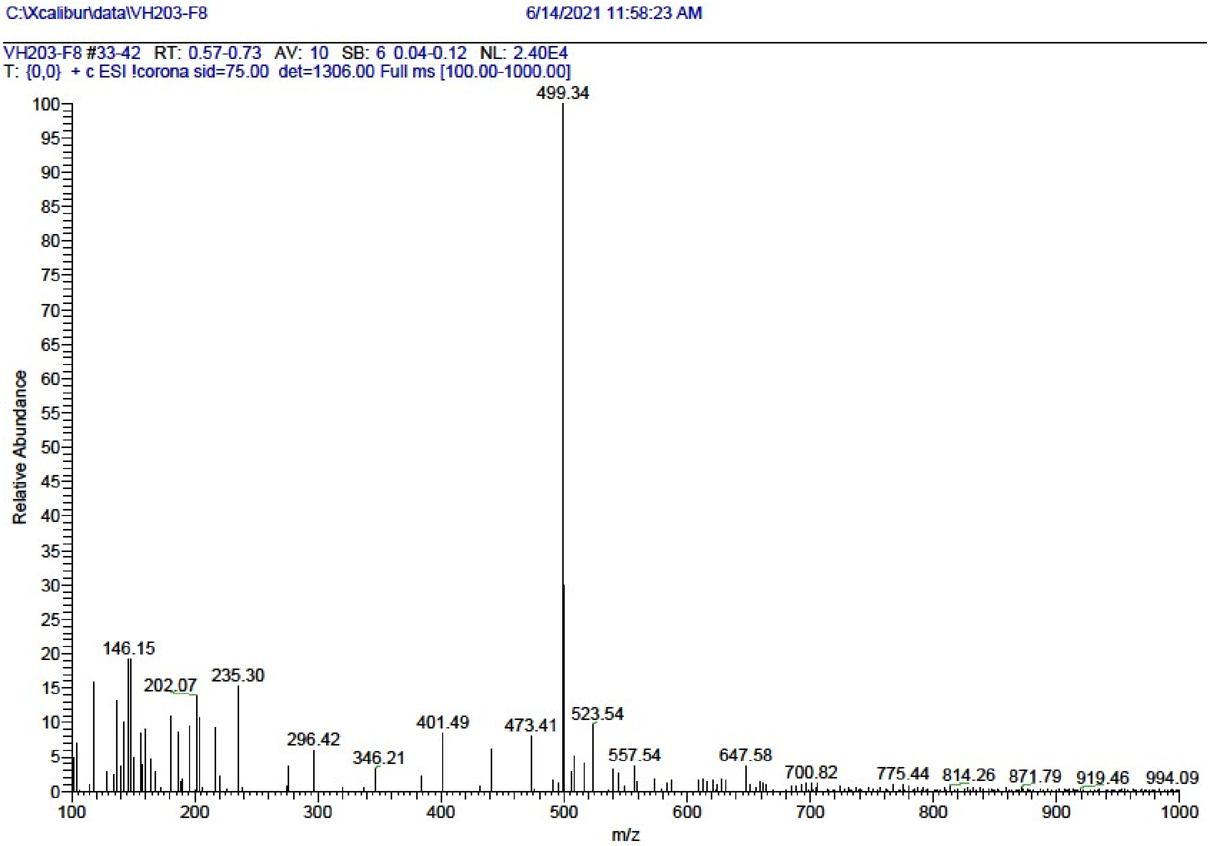

Figure S37: ESI mass spectrum of the photoproduct of (DMA)$_2$F-OAc at 51 min.

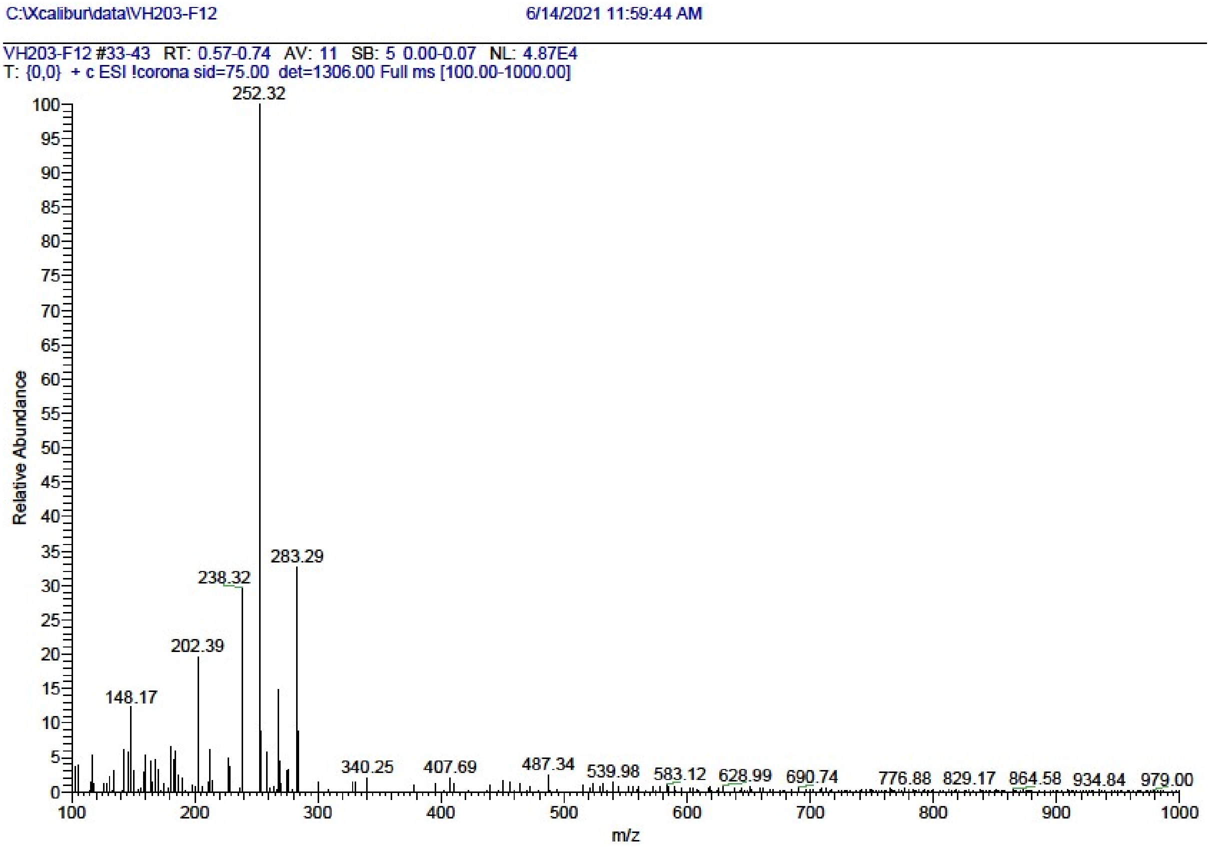

Figure S38: ESI mass spectrum of the photoproduct of $(DMA)_2F$-OH at 15 min.

References

1 C. Slavov, H. Hartmann and J. Wachtveitl, *Anal. Chem.*, 2015, **87**, 2328–2336.

2 M. J. Frisch, G. W. Trucks, H. B. Schlegel, G. E. Scuseria, M. A. Robb, J. R. Cheeseman, G. Scalmani, V. Barone, G. A. Petersson, H. Nakatsuji, X. Li, M. Caricato, A. V. Marenich, J. Bloino, B. G. Janesko, R. Gomperts, B. Mennucci, H. P. Hratchian, J. V. Ortiz, A. F. Izmaylov, J. L. Sonnenberg, D. Williams-Young, F. Ding, F. Lipparini, F. Egidi, J. Goings, B. Peng, A. Petrone, T. Henderson, D. Ranasinghe, V. G. Zakrzewski, J. Gao, N. Rega, G. Zheng, W. Liang, M. Hada, M. Ehara, K. Toyota, R. Fukuda, J. Hasegawa, M. Ishida, T. Nakajima, Y. Honda, O. Kitao, H. Nakai, T. Vreven, K. Throssell, J. A. Montgomery, Jr., J. E. Peralta, F. Ogliaro, M. J. Bearpark, J. J. Heyd, E. N. Brothers, K. N. Kudin, V. N. Staroverov, T. A. Keith, R. Kobayashi, J. Normand, K. Raghavachari, A. P. Rendell, J. C. Burant, S. S. Iyengar, J. Tomasi, M. Cossi, J. M. Millam, M. Klene, C. Adamo, R. Cammi, J. W. Ochterski, R. L. Martin, K. Morokuma, O. Farkas, J. B. Foresman, and D. J. Fox, Gaussian, Inc., Wallingford CT, 2016.

3 A. D. Becke, *Phys. Rev. A*, 1988, **38**, 3098.

4 C. Lee, W. Yang and R. G. Parr, *Phys. Rev. B*, 1988, **37**, 785.

5 T. H. Dunning, *J. Chem. Phys.*, 1989, **90**, 1007–1023.

6 J. Tomasi, B. Mennucci and R. Cammi, *Chem. Rev.*, 2005, **105**, 2999–3093.

7 B. Mennucci, *Wiley Interdiscip. Rev. Comput. Mol. Sci.*, 2012, **2**, 386–404.

8 M. Caricato, B. Mennucci, J. Tomasi, F. Ingrosso, R. Cammi, S. Corni and G. Scalmani, *J. Chem. Phys.*, 2006, **124**, 1–13.

9 B. Lunkenheimer and A. Köhn, *J. Chem. Theory Comput.*, 2013, **9**, 977–994.

10 Q. Sun, X. Zhang, S. Banerjee, P. Bao, M. Barbry, N. S. Blunt, N. A. Bogdanov, G. H. Booth, J. Chen, Z.-H. Cui, J. J. Eriksen, Y. Gao, S. Guo, J. Hermann, M. R. Hermes, K. Koh, P. Koval, S. Lehtola, Z. Li, J. Liu, N. Mardirossian, J. D. McClain, M. Motta, B. Mussard, H. Q. Pham, A. Pulkin, W. Purwanto, P. J. Robinson, E. Ronca, E. R. Sayfutyarova, M. Scheurer, H. F. Schurkus, J. E. T. Smith, C. Sun, S.-N. Sun, S. Upadhyay, L. K. Wagner, X. Wang, A. White, J. D. Whitfield, M. J. Williamson, S. Wouters, J. Yang, J. M. Yu, T. Zhu, T. C. Berkelbach, S. Sharma, A. Y. Sokolov and G. K.-L. Chan, *J. Chem. Phys.*, 2020, **153**, 24109.

11 M. F. Herbst, M. Scheurer, T. Fransson, D. R. Rehn and A. Dreuw, *Wiley Interdiscip. Rev. Comput. Mol. Sci.*, 2020, **10**, 1–16.